Modelling of a wind-wave floating and semi-submersible power plant

Voltá I Roqueta, Laura; Thomas, Sarah; Schmidt Paulsen, Uwe

Published in:
Journal of Physics: Conference Series

Link to article, DOI:
10.1088/1742-6596/1618/5/052032

Publication date:
2020

Document Version
Publisher's PDF, also known as Version of record

Modelling of a wind-wave floating and semi-submersible power plant

Modelling of a wind-wave floating and semi-submersible power plant

Laura Voltá I Roqueta[1], Sarah Thomas[2] and Uwe Schmidt Paulsen[1]

[1]DTU Wind Energy, Risø Campus, Frederiksborgvej 399, DK-4000 Roskilde, Denmark
[2]Floating Power Plant, Park Allé 382, DK-2625 Vallensbæk, Denmark

E-mail: lviro@dtu.dk, st@floatingpowerplant.com, uwpa@dtu.dk

Abstract. This paper exposes a method of modelling and analysis to help verifying design iterations of non-cylindrical shaped floating wind technologies. In order to do so, the Morison based quadratic hydrodynamic drag forcing contribution within the HAWC2-WAMIT coupled model, is modified to account for a panel-based input geometry. The implementation is applied to the P80 platform, and a verification of the hydrodynamic responses is performed. A reduced load case analysis is carried out, in which floating wind technologies can be assessed efficiently during early stage design iterations. The final platform assessment includes the wind and wave coupled effect using three load cases from IEC 61400-3 standards. The results of the simulations show that the chosen cases provide significant information relating to the platform motions and the tower top acceleration, in order to provide feedback for later design iterations of the platform.

1. Introduction

In 2019, Europe installed 15.4 GW of new wind power capacity, 23.4% corresponding to offshore (1). Normally, offshore wind turbines take advantage of better wind resources than their onshore counterparts, achieving significantly more full-load hours (2). After certain water depths, floating wind concepts are forecast to be more economically attractive and benefit from having a smaller visual and acoustic impact (3). Currently, there are several competing design types of Floating Offshore Wind (FOW), but there is not a unique design. For example, there is Equinor's spar buoy type concept, which under the project name Hywind, in 2017 was the world's first multi-unit FOW farm commissioned in Scotland with five 6MW turbines. IDEOL also developed a patented concept under the name of Damping Pool®, which is a barge type, and the Windfloat foundation from Principal Power, is a semi-submersible type. The concept used as a case study in this paper is Floating Power Plant's P80 device. The P80 device is a semi-submersible technology with Wave Energy Converters (WEC) integrated into the floating platform.

The floating wind industry is still in the early stages of development, however there already exist specific standards to which technology developers should adhere (4). Included withing these standards is an extensive list of design load cases for which simulations should be performed using aero-hydro-elastic coupled models. FAST, Bladed and HAWC2 are examples of existing software capable of modeling such designs, and their performance applied to a floating semi-submersible wind system is compared in the offshore Code Comparison Collaboration OC4 phase II (5).

The list of design load cases is comprehensive and should be performed during the detailed design stage of the device development. During the earlier conceptual design phases, simulating the entire list is too time and resource consuming if is to be done for each design iteration. A more lean analysis and design verification process is therefore presented in this paper for use within the conceptual design stage.

The model described in this paper is a HAWC2-WAMIT coupled model, used in (6), but extended to the P80 device and with focus on the hydrodynamic drag modelling.

2. Objectives

The purpose of this work is provide a method of analysis to verify design iterations of non-cylindrical floating wind technologies. To achieve this objective, FPP's P80 device is used as a case study, and two sub-objectives are defined.

(i) Adapt the existing Morison based quadratic hydrodynamic drag forcing contribution on the HAWC2-WAMIT model, so that it is suitable for application in different types of floaters that are not cylindrical-based shaped.

(ii) Develop a methodology to evaluate the stability of the design in an efficient manner.

3. System description and assumptions

The P80 model contains the following components: a semi-submersible platform, the wave energy converters, a wind turbine and a disconnectable turret mooring system (Fig. 1). The concept can carry a single wind turbine ranging from 5 MW to 10 MW, and between 2 MW to 3.6 MW wave power generation converters, depending on the wave resource.

The semi-submersible platform is composed of a central hull, two side pontoons and an aft pontoon. Each of the pontoons contain water ballast and a heave plate at the bottom. The two side pontoons are attached to the central hull by a submerged horizontal plate, referred to as the wave-plate.

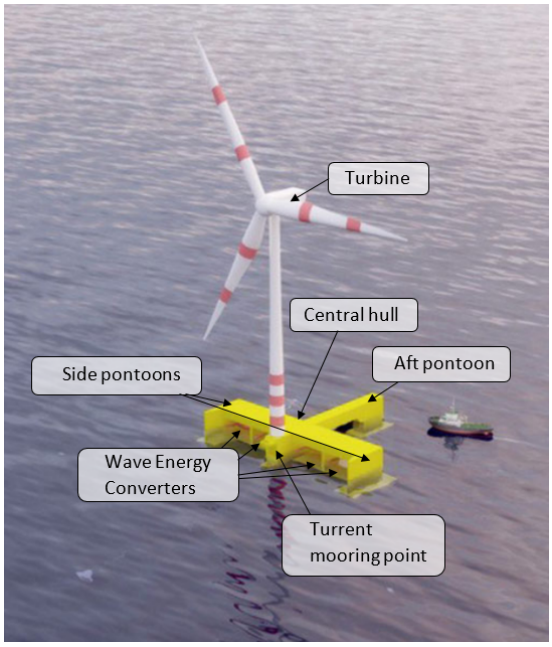

Figure 1. Rendering of the P80 (7).

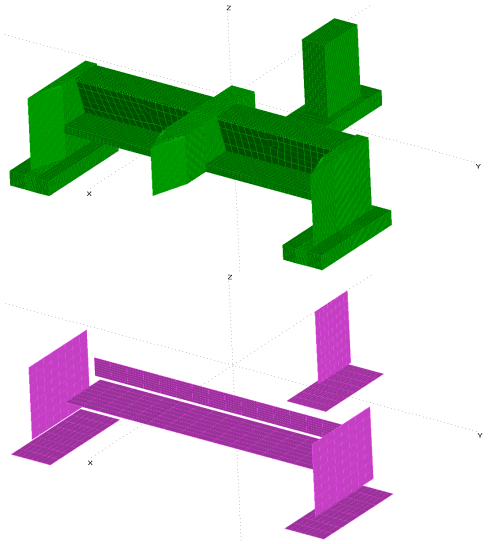

Figure 2. Top: Mesh of the submerged part of the floater, used in WAMIT. Bottom: Floater representation by panel elements used for the quadratic drag calculation in HAWC2.

Integrated into the semi-submersible platform, between the side-pontoons and the central hull, are 4 wave energy converters (WECs). Each WEC consists a wave absorber which oscillates in pitch relative to the platform under the influence of the incoming waves, and hydraulic Power Take-Off (PTO) system. The PTO applies a damping force to the oscillating wave absorber to generate power. Under storm conditions, the absorbers are mechanically locked at a specific angle and do not generate power for safety reasons.

In this paper, the floater is assumed to be a rigid body, and the wave absorbers are fixed in all simulations. Therefore, the system moves as a single floating body. Two different positions of the wave devices are, however, considered as they have an impact on the system dynamics: an operational fixed position to represent the cases when the device is producing wave power, and a survival fixed position which represents cases where extreme waves and wind conditions take place.

The wind turbine and the turret mooring point are located at the fore of the central hull. The platform passively rotates about the turret mooring to face the predominant waves, resulting in a safe leeward wave shelter, whilst the wind turbine yaws to face the predominant wind direction. The technology is therefore subject to misaligned wave, wind and currents. In this paper, however, only heading waves are considered.

The design of the P80 included in this paper is not the final design, but is instead a design iteration designed for a 5MW wind turbine. Determining the extent to which this design is suitable for an 8MW turbine without modification to the semi-submersible design provides an ideal study to reach the paper objectives. Only the external geometry, and an approximate mass distribution when supporting a 5MW wind turbine are given as inputs by the technology developer.

The turbine used in the analysis is an 8 MW down-scaled version of the onshore DTU 10 MW reference wind turbine (8). It is a 3 bladed pitch regulated turbine, with a rotor diameter of 159.5 meters. The rated power is reached at 12 m/s wind speed, and the maximum thrust is about 1200 kN. The turbine structural characteristics have not been adapted for the floating concept, but the DTU Wind Energy Controller (9), used in the original HAWC2 turbine model, has been tuned in order to be suitable for the floating system and avoid a negative aerodynamic damping. The frequency of the controller has been tuned to lie between the first tilt frequency of the platform (pitch) and the first translation mode.

4. Methodology

The frequency-dependent hydrodynamic information and loads of the floater, both from the incoming waves (diffraction) and from the movement of the structure (radiation), is provided by the technology developer in the form of output data from WAMIT® (10), an advanced software for analyzing wave interactions with offshore platforms and other structures, that uses an accurate submerged geometry of the platform (see figure 2). The overall mass distribution for the technology when supporting a 5MW wind turbine, is provided.

In order to obtain a new mass distribution where the 8MW wind turbine is instead installed, both the draft and the total mass distribution are assumed to be unchanged. The extent to which this mass distribution could be achieved by redistributing the ballast water in the semi-submersible platform, is not considered in this paper. By means of a direct convolution, the WAMIT outputs are coupled to the aero-hydro-elastic and non-linear time domain simulation tool HAWC2 (11), to have a HAWC2-WAMIT (6) complete model (Fig. 3). As WAMIT is a linearised potential flow solver, linear wave theory is applied for all the calculations. To reduce the amplitudes of motion close to the resonant frequencies to realistic amplitudes, a quadratic hydrodynamic drag forcing contribution is included internally through HAWC2.

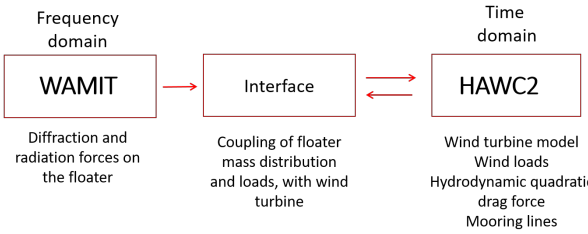

Figure 3. HAWC2-WAMIT coupled system methodology representation

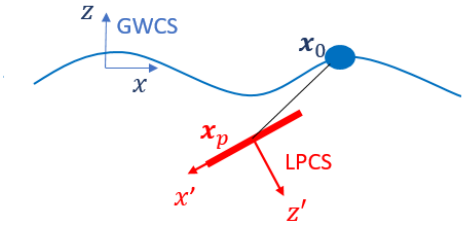

Figure 4. Global WAMIT coordinate system (GWCS) and local panel coordinate systems (LPCS) description.

4.1. Implementation of Quadratic Damping

The Morison drag formulation in HAWC2 is based on cylindrical beam elements, where the user specifies the diameter and the axial and radial coefficients, among others. Nevertheless, with the HAWC2-WAMIT coupled model, the floater mass and inertia terms are exclusively provided by the technology developer and WAMIT. Hence, only the drag coefficient and area are required. However, as described in section 2, the formulation using beams is not suitable for non-cylindrical floater geometries. Hence, another formulation to include the quadratic hydrodynamic drag forcing contribution, has been incorporated in the model. The formulation applies the quadratic drag term of the Morison's equation, to infinitesimally thin rectangular panels (2D) which describe the key surfaces of the floater geometry, as shown in figure 2. Each surface is composed by various panels, each of them having a centroid used for the force calculation. As the panel is infinitesimally thin, it only has an area in a 2D plane.

The description of the implementation is as follows: consider a single infinitesimally thin drag panel which, at a specific time-step, has its centroid at position $\boldsymbol{r}$ in the global WAMIT coordinate system, GWCS (see Fig. 4). The platform motion is always referred at the interface node used for the HAWC2-WAMIT coupling, $\boldsymbol{x}_O$, which is defined at the midpoint and at the centreline of the platform side pontoon and central hull respectively, and at the sea water level (SWL) elevation. Originally, in equilibrium, $\boldsymbol{x}_O$ is located at the GWCS. The local, body-fixed, coordinate system for this panel, LCSP, has its axes parallel and perpendicular to the its surface, as shown also in Fig. 4. To transform coordinates from the local panel coordinates to the global WAMIT coordinate system, a transformation matrix, $\boldsymbol{A}$ is used. It is defined such that $\boldsymbol{d} = \boldsymbol{A}\boldsymbol{c}$, with $\boldsymbol{c}$ being the rotated vector into $\boldsymbol{d}$ through a rotation characterized by the rotation transformation matrix $\boldsymbol{A}$. Using $\boldsymbol{A}$, the location of the centroid of the panel is calculated in the GWCS, $\boldsymbol{x}_p$, using eq.(1). The relative velocity, $\boldsymbol{v}_{rel}$, between the fluid and the panel e ($\boldsymbol{v}_{fluid}$ and $\boldsymbol{v}_e$), is then calculated at the panel centroid using eq. (2) and eq.(3), which is further transformed to the LPCS using eq.(4). The Morison drag force and moment in each panel, $\boldsymbol{f}_{D_e,l}$ and $\boldsymbol{m}_{D_e,l}$, are then computed using eq.(5) and eq.(6). The drag force in LPCS is then transformed back to the GWCS using eq. (7). Finally, in global coordinates, the total drag force and moment vectors $\boldsymbol{f}_D$, $\boldsymbol{m}_D$, are computed as the sum of each individual's panel drag contribution in eq.(8), where N is the total number of panel elements. In this paper, shear forcing on the panels is neglegted. This methodology is equivalent to the approach of applying the Morisons drag force to the projected area of the panel.

Eq. (1) to (8) below, presents the mathematical formulation of the Morison drag force and moment included in the model.

$$\text{Position of panel element in the GWCS:} \quad \boldsymbol{x}_p = \boldsymbol{x}_O + \boldsymbol{A}\boldsymbol{r}, \tag{1}$$

$$\text{Velocity of the structure at } \boldsymbol{x}_p \text{ the GWCS:} \quad \boldsymbol{v}_e = \dot{\boldsymbol{x}}_{O,trans} + \boldsymbol{A} \cdot \dot{\boldsymbol{x}_{O,rot}} \times \boldsymbol{r}, \tag{2}$$

$$\text{Relative velocity fluid-panel e in the GWCS:} \quad \boldsymbol{v}_{rel} = \boldsymbol{v}_{fluid} - \boldsymbol{v}_e, \tag{3}$$

$$\text{Relative velocity in the LPCS:} \quad \boldsymbol{v}_{rel,l} = \boldsymbol{A}^T \boldsymbol{v}_{rel}, \tag{4}$$

$$\text{Panel drag force in the LPCS:} \quad \boldsymbol{f}_{D_e,l} = \frac{1}{2}\rho C_D A_e \boldsymbol{n} \cdot |\boldsymbol{v}_{rel,l}| \boldsymbol{v}_{rel,l}, \tag{5}$$

$$\text{Drag moment at panel in the GWCS:} \quad \boldsymbol{m}_{D_e} = \boldsymbol{r} \times \boldsymbol{f}_{D_{e,l}}, \tag{6}$$

$$\text{Panel drag force in the GWCS:} \quad \boldsymbol{f}_{D_e} = \boldsymbol{A}\boldsymbol{f}_{D_{e,l}}, \tag{7}$$

$$\text{Total drag force and moments in the GWCS:} \quad \boldsymbol{f}_D = \sum_{e=1}^{N} \boldsymbol{f}_{D_e}, \quad , \boldsymbol{m}_D = \sum_{e=1}^{N} \boldsymbol{m}_{D_e} \tag{8}$$

where, $\dot{\boldsymbol{x}}_{\boldsymbol{O}}$ is the platform velocity, with $\dot{\boldsymbol{x}}_{\boldsymbol{O,trans}}$ being components 1 to 3 (linear velocity) and components 4 to 6 being angular velocities $\dot{\boldsymbol{x}}_{\boldsymbol{O,rot}}$, $\boldsymbol{n}$ is the unit normal of the panel in the local panel coordinate system, A_e and C_D are the panel e area and drag coefficient.

For the current work, only the P80 fully submerged heave plates have been represented by panels (no vertical oriented panels included), so the drag has only been considered in the global vertical direction with a drag coefficient $C_D = 2$.

To validate the hydrodynamic aspects of the HAWC2-WAMIT model, including the new drag formulation, the simulations are run excluding the wind contribution. These results can be directly compared to results from hydrodynamic codes. Response Amplitude Operators (RAOs) resulting from Wadam (from DNV-GL) are provided by FPP from one of their engineering partners for comparison. The Wadam analysis is performed using a linearized quadratic drag component in the vertical direction only, using infinitesimally thin beams but with direction-dependent drag coefficients.

4.2. Efficient Methodology for Initial Design Assessment

The most complete floating wind standards that exist today is IEC 61400-3-2 (4). According to them, analyses should be performed for all of the load cases defined for fixed foundation wind turbines as in IEC 61400-3-1 (12), as well as 8 additional load cases for 4 situations specific to floating wind turbines. Each load case consists a range of conditions to be analysed, with each analysis being performed for multiple seeds, resulting in thousands of simulations.

The main purpose of the coupled analysis during the conceptual design stage, is to have a first overview of how the platform behaves and whether it fulfils the design limits established. The focus has therefore been put on analysing the P80 motions (particularly heave and pitch) and the tower top acceleration reached under both operation and storm conditions. The environmental conditions are limited to heading waves (propagating parallel to the central hull of the platform) with aligned wind.

The final selected cases are three load cases from the IEC 61400-3 standards (12): DLC 1.2, DLC 1.3 and DLC 6.1, described in Table 1. Design Load Cases DLC 1.2, DLC 1.3 represent operational conditions with normal and extreme turbulence, hence the wave absorbers will be at their operational fixed angles (see Section 3) and the wind turbine operational. Fatigue analysis is not studied in this paper. Design Load Case DLC 6.1 represents the situation where the wind turbine is in idle mode and there is extreme sea state. Hence, wave absorbers are in their fixed survival positions.

Table 1. Design load cases description

DLC	Wind turbine configuration	Wave device configuration	Wind condition	Waves
1.2	Operation	Fixed - representing operation	Normal turbulence model	Normal Sea State
1.3	Operation	Fixed - representing operation	Extreme turbulence model	Normal Sea State
6.1	Parked	Fixed - representing parked (survival)	Extreme wind model	Extreme Sea State Hs=Hs50

To be able to compare quantitatively and to contribute better on the platform design evaluation, design limitations are to be set. For the present analyses, a maximum design mean pitch angle and a maximum absolute pitch motion constraint are selected, as well as a constraint on the maximum tower top acceleration of the turbine. These constraints can then be used to reflect on the results of the simulations in regards to analysing the input device design.

The wind characteristics used for the load calculations correspond to the wind turbine class IA, as defined in IEC 61400-1 (13). The average wind speed, the reference wind speed and the reference turbulence intensity are hence 10 m/s, 50 m/s and and 0.16 (-) respectively. The cut in wind speed is 4 m/s and the cut-out is at 25 m/s. The bin size used is 2 m/s and 6 seeds per wind speed are included.

North Scotland site-specific wave conditions have been used, provided by Floating Power Plant.For each significant wave height, two different wave peak periods have been considered and referred as sea state 1 and sea state 2, to better evaluate the influence of the sea state on the platform motion. In parked conditions, as per DLC6.1, the extreme sea state with 50-year recurrence period (H_{50}) has been used.

5. Results of the simulations

It should be noted that all values given in this section are normalised by undisclosed values. This allows for the scientific content to be discussed, without sharing confidential information relating to the P80 technology.

Figure 5 shows the comparison of the heave, surge and pitch RAO of the platform, obtained with HAWC2 and Wadam for both the operation and survival configurations of the wave absorbers. In the HAWC2 model, both the existing hydrodynamic drag calculation using cylindrical beam elements (method 2) and the panel-based implementation referred as method 1, are also indicated for comparison.

For the operation configuration, the surge motion RAO obtained with HAWC2 (top left corner of Figure 5), matches the results obtained with Wadam for both HAWC2 drag implementations. Close to highest heave and pitch motion response, the results obtained using the beam implementation of drag are however considerably different to those calculated using Wadam, and the implementation using panels results in a much better fit. When using the beams method, an axial and a radial drag coefficients are defined together with the corresponding cross sectional areas. In this particular case, this leads to an undesired drag contribution in other directions than the vertical. When the platform is pitching or rolling as a consequence of the platform motion's coupling, the area of the main hull facing the waves will be adding a drag force contribution in the surge direction, and the side pontoons will be adding a force in the sway motion, both as a consequence of using the radial drag coefficient. When using the drag computation based on the panels formulation instead, each panel contributes differently

depending on its orientation, drag coefficient and area, and more accurate platform responses are achieved.

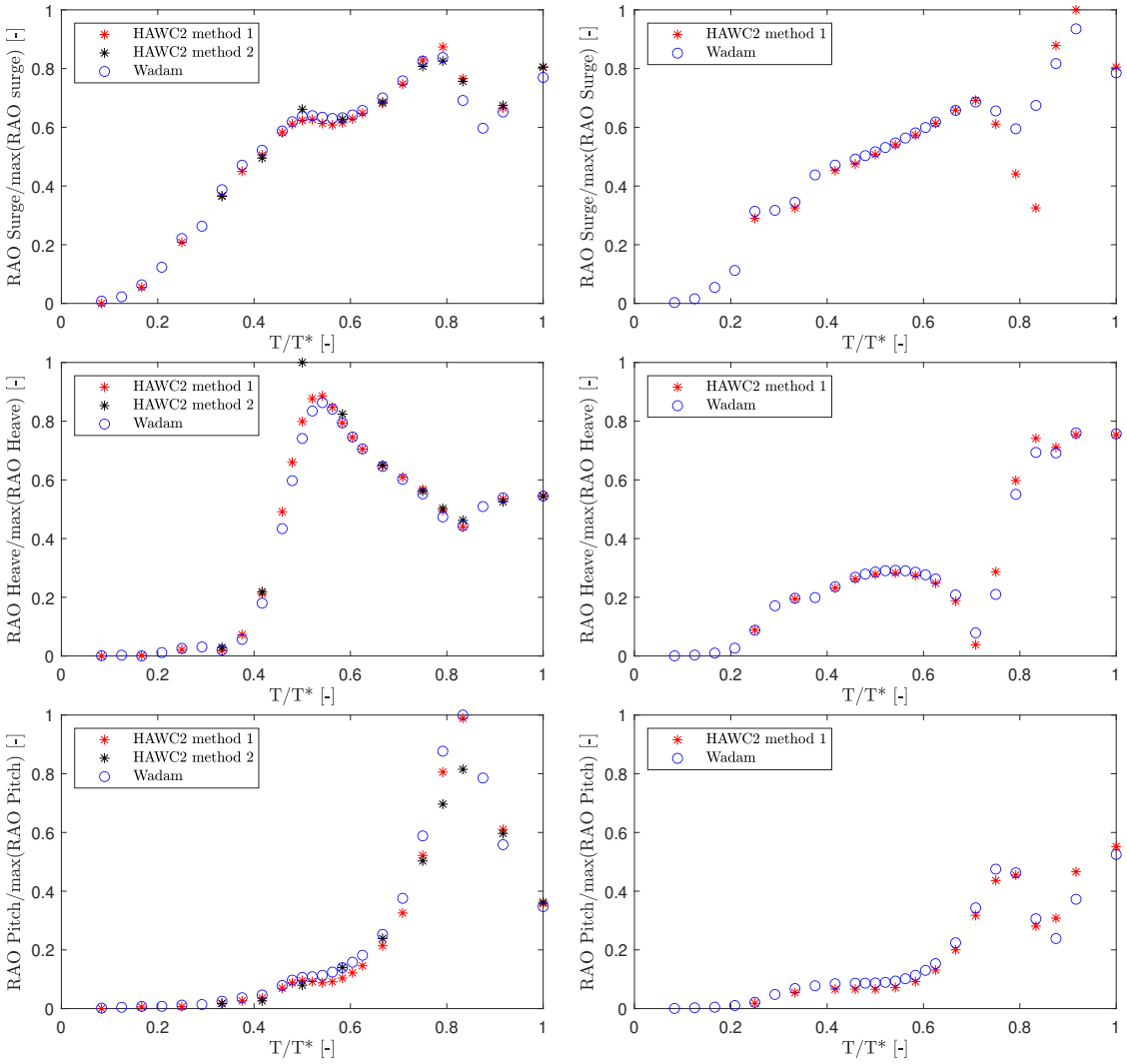

Figure 5. Comparison of the platfom surge (top), heave (middle) and pitch (bottom) RAOs, between WADAM (blue○) and HAWC2, for different wave periods T normalized by the maximum period considered T*. Left: operation configuration. Right: Survival configuration. HAWC2 Method 1 (red*): panel description and direction-dependent drag coefficients. Method 2 (*): cylindrical beams with axial and radial drag coefficients.

Analyzing the influence of the wave absorbers configuration, from Figure 5 it can be seen that there is a clear difference between the operation (left column figures) and the survival (right column figures). Higher heave and pitch platform responses are achieved in operation, while the surge motion is higher for the survival blocked position. Moreover, the excitation of the modes happens at different wave periods for both configurations, during longer waves for the survival configuration. Hence, the platform motions under both configurations are expected to be very different.

Figures 6, 7 and 8 show the platform motion in heave, pitch and the fore-aft tower top acceleration respectively, for the operation cases DLC1.2 (normal wind) and DLC1.3 (extreme

turbulence). The mean value of the heave platform motion (shown in Figure 6) is almost zero in both load cases as a consequence of the oscillation around the still water level. The heave motion is driven by the waves and there is a clear dependency on the sea state and wave period.

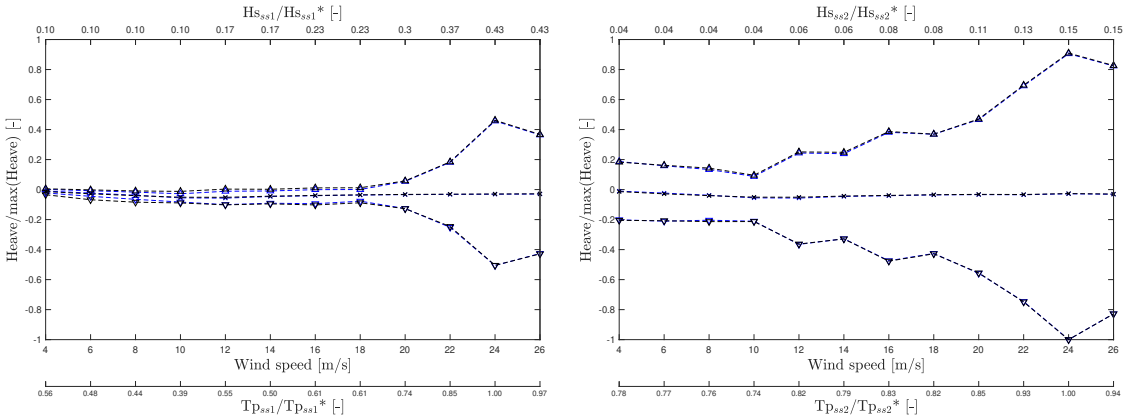

Figure 6. Maximum ($\triangle$), minimum ($\bigtriangledown$) and mean (x) platform heave motion as function of wind speed for both DLC1.2 (blue- - - -)and DLC1.3 (- - - -). The left figure is under sea state 1 (ss1) and the right figure to sea state 2 (ss2), both normalized by the non-disclosed maximum peak period considered Tp$_{ss}$*, and Hs$_{ss}$* being the corresponding Hs at Tp$_{ss}$*.

Sea state 2 from Figure 6, leads to higher platform heave responses than sea state 1 and the deviations from the mean are indeed higher. Nevertheless, under sea state 1 the change in the heave platform response is more aggressive, from nearly zero deviation from the mean at low wind speeds, to a sudden excitation above 20 m/s. In both load cases and for both sea states, there is a maximum occurring at the longest wave condition (highest Tp) and the response seems to be then damped again for larger wind speeds.

The pitch motion, shown in Figure 7, is more dependent on the wind speed. Small differences observed between the two sea states. The motion follows the same pattern as the thrust curve of the turbine, increasing with wind speed up to rated, and decreasing for higher wind speeds. For the extreme turbulence model, DLC1.3, the deviations from the mean are higher than for DLC1.2 as a consequence of a higher turbulence model. Under both load cases, the platform motion is stable and the heave motion excitation doesn't seem to be reflected in the pitch statistics.

The mean tower top acceleration is zero and the amplitude increases almost symmetrically with increasing wind speed. Under DLC1.2, the acceleration is within the design limits established (TT fore-aft acc$_{limit}$) for both sea states, while for DLC1.3, the limit is exceeded in both cases at high wind speeds. Moreover, comparing the influence of the sea states, it can be concluded that sea state one (left of Figure 8) leads to higher accelerations at wind speeds between 18 and 24 m/s than sea state 2. The acceleration limit constrain is indeed exceeded for wind speeds higher than 20 m/s for sea state 1, whereas it is exceeded only from 24 m/s for seas state 2 conditions.

Regarding the storm conditions, the pitch motion is below the maximum design constrain. However, the tower top acceleration in the fore-aft direction, exceeds the limits. This can be observed in the DLC6.1 column of the Table 2, which shows the normalized platform motions and tower top acceleration, for all load cases.

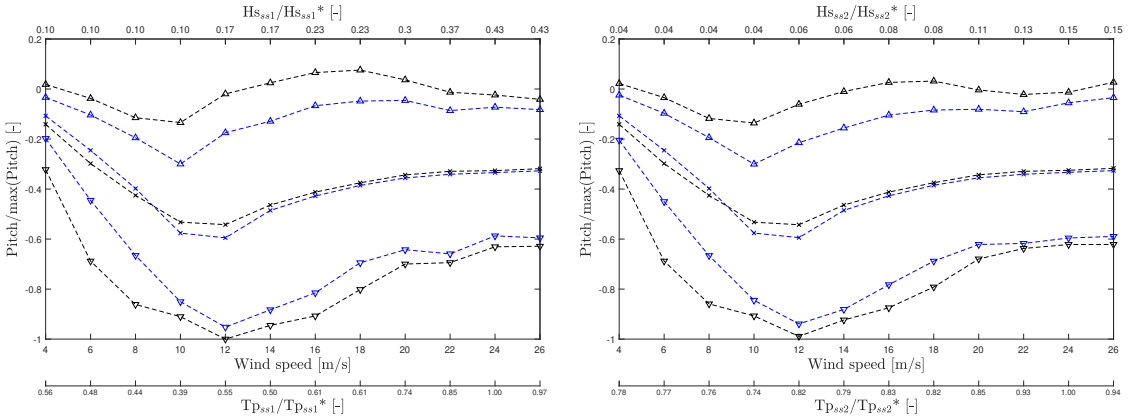

Figure 7. Maximum (△), minimum (▽) and mean (x) platform pitch motion as function of wind speed for both DLC1.2 (blue- - - -)and DLC1.3 (- - - -). The left figure is under sea state 1 (ss1) and the right figure to sea state 2 (ss2), both normalized by the maximum peak period considered, Tp$_{ss}$*, and Hs$_{ss}$* being the corresponding Hs at Tp$_{ss}$*.

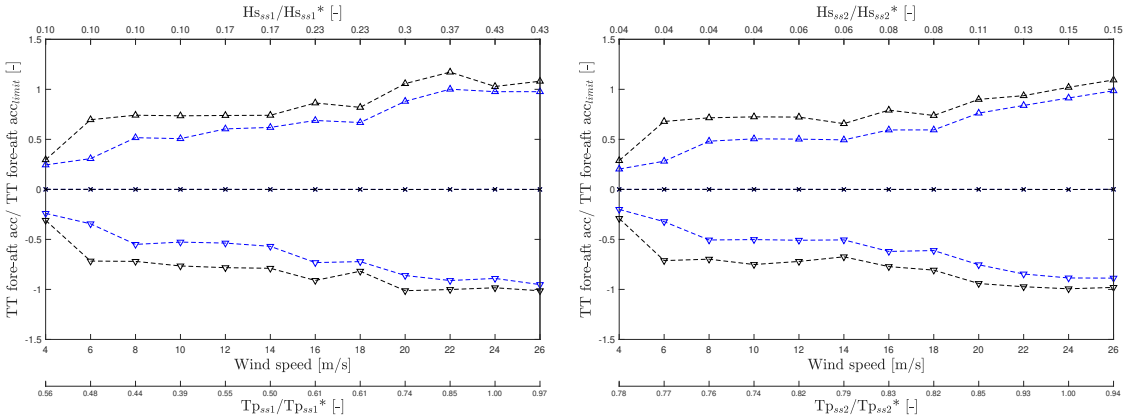

Figure 8. Maximum (△), minimum (▽) and mean (x) tower top fore-aft acceleration as function of wind speed for both DLC1.2 (blue- - - -)and DLC1.3 (- - - -). The left figure is under sea state 1 (ss1) and the Right figure to sea state 2 (ss2), both normalized by the non-disclosed maximum peak period considered Tp$_{ss}$*, and Hs$_{ss}$* being the corresponding Hs at Tp$_{ss}$*.

From table 2, it can be seen that the maximum platform heave and tower top fore-aft acceleration are achieved during storm conditions (DLC6.1), whereas the maximum pitch is achieved during one of the operation conditions under an extreme wind turbulence model (DLC1.3). In storm conditions, the severe sea sate characterized by high wave heights dominates the heave motion. Nevertheless, in that condition the turbine is not operating and the wind thrust is much lower than in operation, which leads to a lower pitch motion of the platform. Figure 9 illustrates, for a better comparison, the time series of a simulation for both DLC1.3 (left figure) where the maximum pitch was achieved, and for DLC6.1(right figure) where a maximum in the tower acceleration is achieved.

Table 2. Comparison of statistics from DLC6.1 and DLC1.2 and 1.3. The normalization is done taking the maximum response among the 3 load cases, and the acceleration limit (TT fore-aft acc_{limit}*) is the established constraint for the storm condition.

Signal	**DLC1.2**		**DLC1.3**		**DLC6.1**
	SS_1	SS_2	SS_1	SS_2	
Heave/max(Heave) [-]	0.446	0.882	0.445	0.882	1.000
Pitch/max(Pitch) [-]	0.952	0.939	1.000	0.989	0.856
TT fore-aft acc/TT fore-aft acc_{limit}* [-]	0.501	0.493	0.586	0.547	1.930

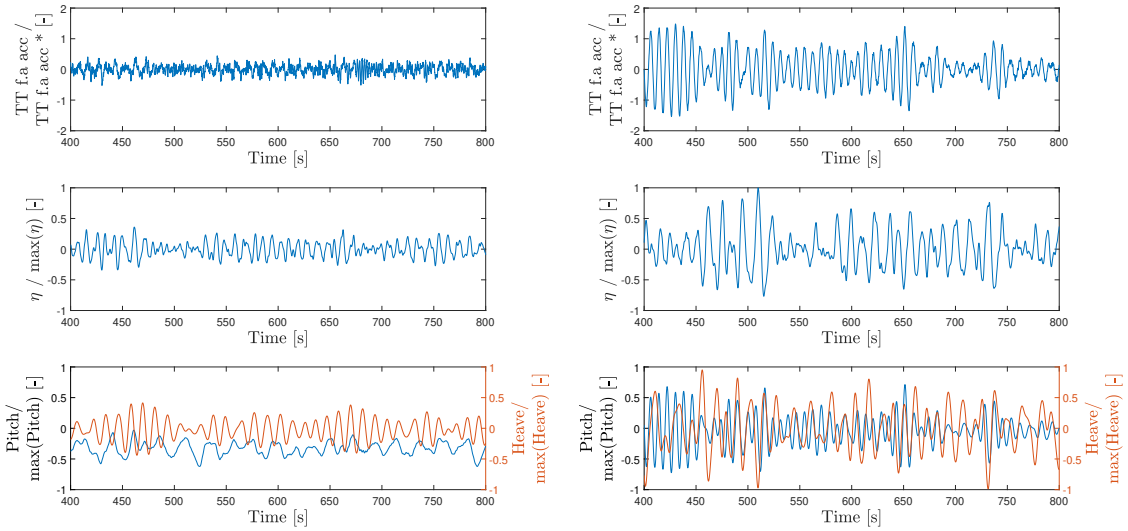

Figure 9. Time series of the tower top acceleration in the for-aft direction (top), the water surface elevation η at free surface level (middle), and the pitch and heave motions of the floater (bottom). Left column: DLC1.3 under sea state 1 conditions and at 24 m/s wind speed. Right column: DLC6.1 for a wind speed at hub height of 50 m/s (Vref) and an extreme sea state with Hs_{50}. TT f.a acc * is taken as the constrain limit.

From Figure 9 (bottom), it can be observed that the heave motion follows the water surface elevation, and there is a coupling between the heave and pitch motion. Both platform motions lead to the tower top fore-aft acceleration response, and when the limit is exceeded, a correlation with higher amplitudes of the platform motions is observed.

6. Conclusions

As the floating wind industry matures, so does the standards to which the technologies must be designed towards. The latest floating wind standards (4) require thousands of simulations to be performed in order to verify the technologies performance and behaviours in a range of relevant scenarios. These simulations require the use of coupled aero-hydro-elastic codes which can simulate the loads and motions of the floating platform together with its mooring and wind turbine in varying wave, wind and current conditions. One such code is HAWC2, that can couple results from the linear, frequency-domain, wave-structure interaction software, WAMIT, to its full aeroelastic non-linear time domain code and adds non-linear hydrodynamic drag force

on top. In the present paper, HAWC2-WAMIT is used and extended to include a quadratic drag formulation based on 2D panels, which have a different drag coefficient representative of the panel direction and area. This modification better suits the code for application to non-cylindrical floating foundations, such as Floating Power Plant's P80 device.

Further to this, a methodology is outlined and implemented to assess a design iteration of a floating wind technology during the concept development phase, without performing thousands of simulations. The methodology requires the definition of design constraints, in this case for maximum mean platform pitch angle and maximum tower acceleration. Simulations for 3 of the 40+ required Design Load Cases are run, and the results are compared against the design constraints.

To validate the hydrodynamic aspects of the HAWC2-WAMIT model, inlcuding the panel-based drag formulation, the simulations are run excluding the wind contribution, and with drag in the global vertical direction only (no vertical panels included). The obtained RAOs of the P80 match closely with results from the commercial hydrodynamic software Wadam, and the implementation is verified for this specific case. To fully test the implementation, future work should include horizontal drag, the use of the vertical panels, and it should be applied and compared to different geometries.

After the evaluation of the design load simulations, it can be concluded that the maximum heave motion of the platform occurs during the survival load case DLC6.1, whereas the maximum platform pitch is achieved during the operation condition DLC1.3. Both motions are coupled, and it has been observed that the tower top acceleration is indeed exceeding the design constraints when heave and pitch reach the highest amplitudes. For that reason, it is believed that the methodology and the chosen design cases were adequate to provide a first feedback to the technology developer for further design iterations of the platform. Nevertheless, it is important to include a wind and wave misaligned case in the platform assessment, as the aerodynamic damping would not always be in the platform pitch direction. The reduced load case analysis presented in this paper should therefore be extended to include a fourth case in which the waves and wind are misaligned. Implementation of such a load case requires all geometry panels to be included.

References

[1] Wind europe `https://windeurope.org/about-wind/statistics/` accessed: 2020-17-02

[2] Ackermann T, Leutz R and Hobohm J 2001 World-wide offshore wind potential and european projects *2001 Power Engineering Society Summer Meeting. Conference Proceedings (Cat. No. 01CH37262)* vol 1 (IEEE) pp 4–9

[3] Castro-Santos L, Filgueira-Vizoso A, Carral-Couce L and Formoso J Á F 2016 *Energy* **112** 868–882

[4] IEC 2019 IEC 61400-3-2:2019 Wind energy generation systems - Part 3-2: Design requirements for floating offshore wind turbines. standard International Electrotechnical Commission Geneva, Switzerland

[5] Robertson A, Jonkman J, Musial W, Vorpahl F and Popko W 2013 Offshore code comparison collaboration, continuation: Phase ii results of a floating semisubmersible wind system Tech. rep. National Renewable Energy Lab.(NREL), Golden, CO (United States)

[6] Bellew S, Yde A and Verelst D R 2014 Application of the aero-hydro-elastic model, hawc2-wamit, to offshore data from floating power plants hybrid wind-and wave-energy test platform, p37 *5th International Conference on Ocean Energy* (Marine Renewables Canada)

[7] Floating power plant `http://www.floatingpowerplant.com/` accessed: 2019-13-01

[8] Bak C, Zahle F, Bitsche R, Kim T, Yde A, Henriksen L, Hansen M, Blasques J, Gaunaa M and Natarajan A 2013 The dtu 10-mw reference wind turbine

[9] Hansen M and Henriksen L 2013 *Basic DTU Wind Energy controller* (*DTU Wind Energy E* no 0028) (Denmark: DTU Wind Energy)

[10] Lee C and Newman J 2013 *WAMIT, Inc., Chestnut Hill, MA*

[11] Larsen T and Hansen A 2007 *How 2 HAWC2, the user's manual* (*Denmark. Forskningscenter Risoe. Risoe-R* no 1597(ver. 3-1)(EN)) (Risø National Laboratory) ISBN 978-87-550-3583-6

[12] IEC 2019 IEC 61400-3-1:2019 Wind energy generation systems - Part 3-1: Design requirements for fixed offshore wind turbines. standard International Electrotechnical Commission Geneva, Switzerland

[13] IEC 2019 IEC 61400-1 Ed4: Wind turbines - Part 1: Design requirements. standard International Electrotechnical Commission Geneva, Switzerland